

# Nanoscale

Accepted Manuscript



This is an *Accepted Manuscript*, which has been through the Royal Society of Chemistry peer review process and has been accepted for publication.

*Accepted Manuscripts* are published online shortly after acceptance, before technical editing, formatting and proof reading. Using this free service, authors can make their results available to the community, in citable form, before we publish the edited article. We will replace this *Accepted Manuscript* with the edited and formatted *Advance Article* as soon as it is available.

You can find more information about *Accepted Manuscripts* in the [Information for Authors](#).

Please note that technical editing may introduce minor changes to the text and/or graphics, which may alter content. The journal's standard [Terms & Conditions](#) and the [Ethical guidelines](#) still apply. In no event shall the Royal Society of Chemistry be held responsible for any errors or omissions in this *Accepted Manuscript* or any consequences arising from the use of any information it contains.



## Anisotropic Photocurrent Response at Black Phosphorous-MoS<sub>2</sub> p-n Heterojunctions

Tu Hong,<sup>a</sup> Bhim Chamlagain,<sup>b</sup> Tianjiao Wang,<sup>a</sup> Hsun-Jen Chuang,<sup>b</sup> Zhixian Zhou,<sup>\*b</sup> and Ya-Qiong Xu<sup>\*a, c</sup>

Received 00th January 20xx,  
Accepted 00th January 20xx

DOI: 10.1039/x0xx00000x

[www.rsc.org/](http://www.rsc.org/)

We investigate the photocurrent generation mechanisms at a vertical p-n heterojunction between black phosphorus (BP) and molybdenum disulfide (MoS<sub>2</sub>) flakes through polarization-, wavelength-, and gate-dependent scanning photocurrent measurements. When incident photon energy is above the direct band gap of MoS<sub>2</sub>, the photocurrent response demonstrates a competitive effect between MoS<sub>2</sub> and BP in the junction region. In contrast, if the incident photon energy is below the band gap of MoS<sub>2</sub> but above the band gap of BP, the photocurrent response at the p-n junction exhibits the same polarization dependence as that at the BP-metal junction, which is nearly parallel to the MoS<sub>2</sub> channel. This result indicates that the photocurrent signals at the MoS<sub>2</sub>-BP junction primarily result from the direct band gap transition in BP. These fundamental studies shed light on the knowledge of photocurrent generation mechanisms in vertical 2D semiconductor heterojunction junctions, offering a new way of engineering future two-dimensional materials based optoelectronics devices.

### Introduction

Heterostructures based on two-dimensional (2D) materials have evolved into a thriving research field in the past few years. While the in-plane covalent bonds provide strong connections within each layer, van-der-Waals-like forces bond different layers together, enabling the artificial stacking of 2D crystals on top of each other without the constraint of atomic commensurability. This vertical integration of layered materials has opened up new horizons for future optoelectronic devices such as photovoltaics, light-emitting diodes, and photodetectors.<sup>1-5</sup> By choosing 2D materials with different band gaps and workfunctions, vertical heterostructures with tunable carrier concentrations can be precisely engineered to meet specific needs.<sup>1, 6</sup> In particular, van der Waals heterostructures consisting of transition metal dichalcogenides (TMDCs) are ideal candidates due to their unique optical properties and strong light-material interactions.<sup>7-11</sup> For example, 2D p-n heterojunctions can be realized by simply stacking two TMDC materials together.<sup>6, 12-14</sup> In contrast to conventional chemically doped p-n homojunctions, this 2D structure provides an abrupt transition between the p-type and the n-type materials while concerns of lattice mismatches between materials are eliminated,<sup>5</sup> offering new possibilities for designing semiconductor devices.

Recently, black phosphorous (BP) has been demonstrated as a novel 2D material for electronics and optoelectronics.<sup>15-18</sup> While the band gap of bulk BP is 0.3 eV, its few-layer structures have a thickness-dependent direct band gap ranging from 0.3 eV to 2 eV.<sup>19-22</sup> Few-layer BP based field-effect transistor and phototransistor have been demonstrated to have a mobility up to 10000 cm<sup>2</sup>/V·s and photoresponsivity up to 4.8 mA/W, respectively.<sup>15, 17, 23</sup> By stacking few-layer BP and molybdenum disulfide (MoS<sub>2</sub>), a vertical p-n junction can be built to achieve a maximum photocurrent response of 418 mA/W,<sup>13</sup> much larger than the photoresponsivity of photodetectors based on only BP or MoS<sub>2</sub>.<sup>24-26</sup> To further improve its photoresponsivity, it is important to investigate the photocurrent generation mechanisms of this novel heterostructure.

Here, we demonstrate a vertical p-n heterojunction between BP and MoS<sub>2</sub> flakes. The photocurrent response at this p-n junction has been investigated through spatially resolved photocurrent measurements. If the photon energy is above the direct band gap of MoS<sub>2</sub>, the photocurrent signal at the p-n junction shows a competitive effect between BP and MoS<sub>2</sub>. In contrast, upon 1550 nm laser illumination, the maximum photocurrent occurs when the excitation laser is polarized nearly along the MoS<sub>2</sub> channel (or perpendicular to the BP channel), similar to the photoresponse behaviour at the BP-metal junction. This result indicates that the relatively low energy photons can only excite the electrons in the valence band of BP into its conduction band, which are subsequently injected into the MoS<sub>2</sub> channel to induce photocurrent signals at the junction.

<sup>a</sup> Department of Electrical Engineering and Computer Science, Vanderbilt University, Nashville, TN, USA.

<sup>b</sup> Department of Physics and Astronomy, Wayne State University, Detroit, MI, USA.

<sup>c</sup> Department of Physics and Astronomy, Vanderbilt University, Nashville, TN, USA.

\* Address correspondence to [yqiong.xu@vanderbilt.edu](mailto:yqiong.xu@vanderbilt.edu) and [xzzhou@wayne.edu](mailto:xzzhou@wayne.edu).

## Results and discussion

To fabricate BP-MoS<sub>2</sub> junction devices, MoS<sub>2</sub> thin flakes were first mechanically exfoliated from a bulk MoS<sub>2</sub> crystal onto a degenerately doped 290 nm SiO<sub>2</sub>/Si substrate, while BP flakes were mechanically exfoliated from a BP crystal onto a PDMS stamp. Next, a selected BP thin flake on the PDMS stamp was placed on top of a selected MoS<sub>2</sub> flake on the SiO<sub>2</sub>/Si substrate to form a BP-MoS<sub>2</sub> heterojunction in the overlap region using a home-built precision transfer stage. Finally, metal electrodes were defined by electron beam lithography and subsequent deposition of 5 nm Ti and 40 nm Au. Figure 1a shows the schematic illustration of a BP-MoS<sub>2</sub> junction device along with its optical image. The thickness of the MoS<sub>2</sub> and BP layers are 4.8 nm and 10.0 nm, respectively, as determined by Park-Systems XE-70 noncontact atomic force microscopy. In each MoS<sub>2</sub> layer, hexagonally packed molybdenum atoms are sandwiched between two layers of sulphur atoms,<sup>9</sup> whereas each phosphorous atom is bonded with three neighbouring atoms to form a puckered layer (Figure 1b).<sup>27</sup> We measure the electrical property of the junction in high vacuum ( $\sim 10^{-6}$  torr) with the gate voltage  $V_g$  applied to the Si substrate to adjust the carrier concentration in each material. Figure 1c presents the gate-dependent transport characteristics of the individual MoS<sub>2</sub> and BP layers while its semilog plot is shown in the inset. At zero gate bias, the MoS<sub>2</sub> and BP flakes display n-type and p-type characteristics, respectively, forming a p-n junction in the overlap region. As the gate voltage increases to 60 V, the BP crystal becomes n-doped whereas the MoS<sub>2</sub> layers witness an elevated electron concentration. The mobility values of MoS<sub>2</sub> and BP are estimated to be  $\sim 43$  cm<sup>2</sup> V<sup>-1</sup> s<sup>-1</sup> and  $\sim 38$  cm<sup>2</sup> V<sup>-1</sup> s<sup>-1</sup>, respectively. The I-V characteristics of the BP-MoS<sub>2</sub> junction

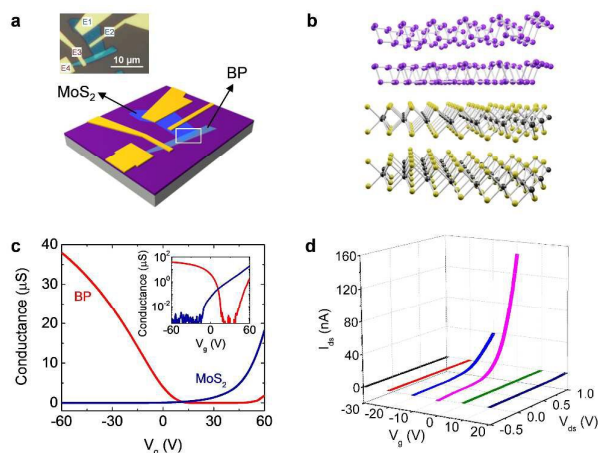


**Figure 1.** (a) Schematic illustration of a BP-MoS<sub>2</sub> p-n junction. The junction area is marked by the white rectangle. Top: optical image of the junction. The electrodes are defined as E1 – E4 as marked in the image. (b) Schematic illustration of the crystal structure of the junction. (c) Gate-dependent transport characteristics for BP (red curve, measured between E3 and E4) and MoS<sub>2</sub> (blue curve, measured between E1 and E2) at  $V_{ds} = 100$  mV, respectively. Inset: the same gate-dependent transport characteristics in a semilog plot. (d) I-V curves at various gate voltages measured between E2 and E3.

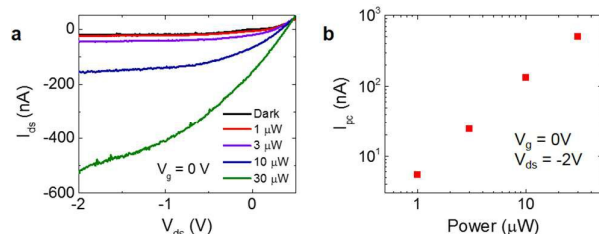


**Figure 2.** (a) I-V characteristics of the BP-MoS<sub>2</sub> p-n junction in dark state and under 532 nm laser illumination. No gate bias was applied. (b) Power dependence of photocurrent intensities in the junction region.

measured between electrode E2 and E3 are shown in Figure 1d at various gate voltages. Consistent with the gate-tunable transport curves, the unintentional doping at zero gate bias allows for strong rectification of drain current. This rectification ratio reduces when the carrier concentrations in the junction region are electrostatically modified. Although the observed I-V characteristics are similar to conventional p-n junctions, the electronic tunability of vertical p-n heterostructures are likely to be attributed to tunnelling-assisted interlayer recombination due to the absence of a depletion region.<sup>6</sup>

Besides the transport characteristics of the BP-MoS<sub>2</sub> p-n heterojunction, we explore its optoelectronic properties. A diffraction-limited 532 nm (2.33 eV) laser spot was focused in the p-n junction area to evaluate its performance in photocurrent response under drain bias. The size of the laser spot is about 1  $\mu$ m, which is much smaller than the BP-MoS<sub>2</sub> overlapped region. The photon energy is above the direct band gap of both few-layer MoS<sub>2</sub> ( $\sim 1.9$  eV) and BP (0.3 eV), providing high efficiency of photocurrent generation.<sup>28</sup> Figure 2a presents the I-V characteristics of the p-n junction in dark state and under various laser illumination intensities in the reverse bias region from  $-2$  V to 0.5 V. At  $V_g = 0$  V, the photocurrent  $I_{pc}$  (defined as  $I_{illumination} - I_{dark}$ ) generated at the p-n junction strongly depends on both drain bias and incident laser power. The highest photoresponsivity is  $\sim 170$  mA/W at  $V_{ds} = -2$  V and 30  $\mu$ W laser power, which is comparable to the photoresponsivity at a BP-MoS<sub>2</sub> p-n junction in a previous report<sup>13</sup> and nearly 40 times higher than the reported BP phototransistors.<sup>15</sup> As shown in Figure 2b,  $I_{pc}$  has a superlinear relationship with increasing laser power at a reverse drain bias, which is possibly due to nonequilibrium occupancy of intragap recombination centers at low laser powers.<sup>29</sup>

Moreover, scanning photocurrent microscopy was utilized to obtain spatially-resolved photocurrent mapping of the BP-MoS<sub>2</sub> device to investigate the photocurrent generation process. In our experiments, a diffraction-limited 785 nm laser spot was scanned over the sample by a piezo-controlled mirror with nanometer-scale spatial resolution. Figure 3a shows the reflection image of the p-n junction between BP and MoS<sub>2</sub> flakes, where the edges of the electrodes are marked by grey dashed lines. The blue and purple dashed lines in these

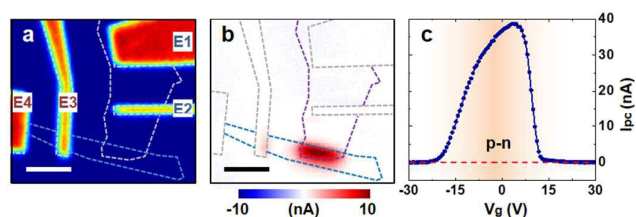


**Figure 3.** (a) The reflection and (b) scanning photocurrent images of the BP-MoS<sub>2</sub> p-n junction (measured between E2 and E3) under zero-gate bias. The light dashed lines mark the position of the electrode, whereas the blue and purple dashed lines mark the outline of the BP crystal and MoS<sub>2</sub> crystal, respectively. (c) The photocurrent intensity in the p-n junction region as a function of gate voltage. The scale bars are 4  $\mu$ m and illumination wavelength is 785 nm.

images outline BP and MoS<sub>2</sub> crystals, respectively. At zero gate bias, a p-n junction is formed at the BP-MoS<sub>2</sub> interface, leading to strong electron-hole pair separation at the junction. Separated electron-hole pairs induce remarkable photocurrent signals (Figure 3b), which can be suppressed when modulating the electrostatic gating in either the positive or negative direction (Figure 3c). This result may be attributed to the increase of the interlayer recombination rate due to the accumulation of one type of majority carriers.<sup>5</sup> In addition, electrostatic gating can also modulate the built-in electric field at the MoS<sub>2</sub>-BP interface, which may also contribute to the gate-dependent photocurrent.

To further explore the relative contributions of different photocurrent generation mechanisms to the overall photocurrent response, we performed polarization-dependent photocurrent measurements of the BP-MoS<sub>2</sub> p-n junction under laser illumination with different wavelengths. The direction of the polarization is defined as shown in Figure 4a, where 0° and 90° denote the directions parallel to the edge of electrodes at MoS<sub>2</sub> and BP sides, respectively. As shown in Figure 4b, when the BP-MoS<sub>2</sub> p-n heterojunction is excited by 532 nm laser, the photocurrent signals are maximized when the laser polarization direction is perpendicular to the MoS<sub>2</sub> channel or nearly along the edge of electrodes on the MoS<sub>2</sub> side (-30°). The photocurrent response at the metal contacts with 532 nm illumination can hardly be identified. These signals may be overshadowed by the strong photocurrent response at the junction region. Interestingly, the photocurrent response displays a different signature under 1550 nm illumination, where the maximum photocurrent signals are observed when the laser polarization direction is perpendicular to the electrode edges on the MoS<sub>2</sub> side (90°) and parallel to the electrode edges on the BP side (Figure 4c and 4d). Raman spectroscopy was performed to determine the orientation of the BP flake.<sup>30</sup> The x direction of BP is at about 30°, indicating the intrinsic anisotropy of BP absorption does not dominate the polarization-dependent photocurrent generation at the junction.

Different polarization dependences of the photocurrent

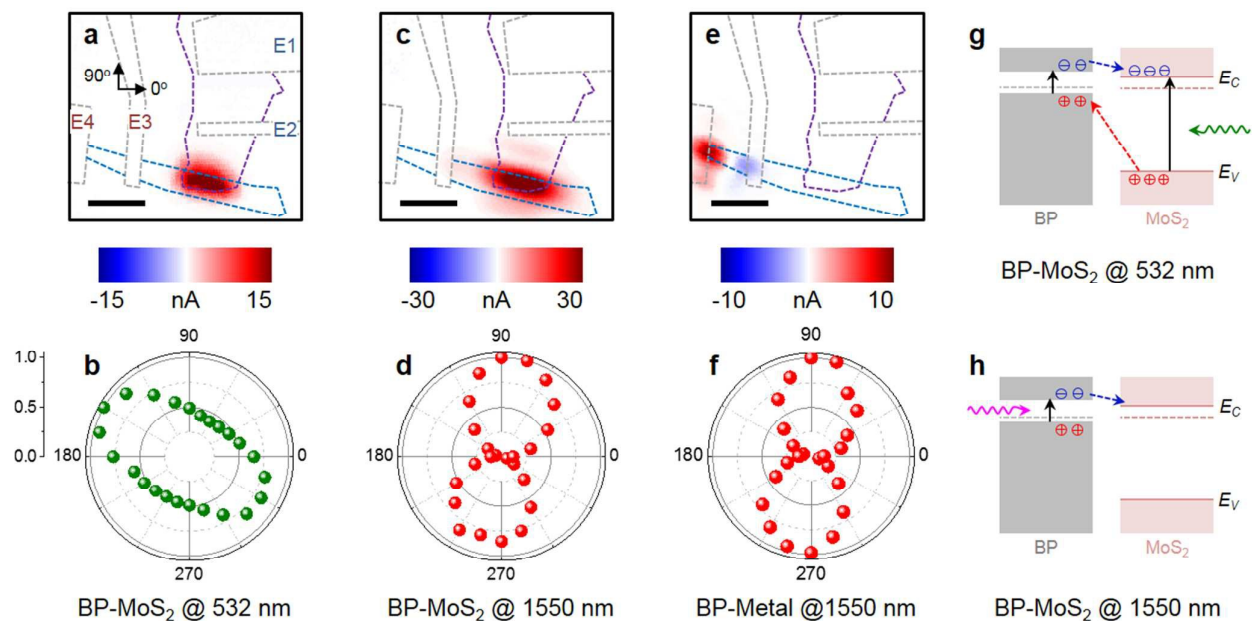


**Figure 4.** Photocurrent images of the BP-MoS<sub>2</sub> junction upon illumination with different wavelength (measured between E1 and E4 electrodes): (a) 532 nm and (c) 1550 nm. The direction of 0° and 90° are defined as marked in the image, where 0° is the direction parallel to MoS<sub>2</sub> electrode edge. Normalized photocurrent intensities in the BP-MoS<sub>2</sub> p-n junction area when illuminated with linearly-polarized (b) 532 nm and (d) 1550 nm laser. (e) Photocurrent image and (f) normalized photocurrent intensity at the BP-metal junction (measured between E3 and E4 electrodes). Schematic diagrams show photocurrent generation mechanisms when the junction is excited by (g) 532nm laser and (h) 1550 nm laser, respectively. The scale bars are 4  $\mu$ m. The powers for 532 nm and 1550 nm lasers are 1  $\mu$ W and 35  $\mu$ W, respectively.

response at the BP-MoS<sub>2</sub> are attributed to different photocurrent generation mechanisms. As shown in Figure 4g, when the BP-MoS<sub>2</sub> junction is excited by 532 nm (2.33 eV) laser, the electrons in the valence bands of both MoS<sub>2</sub> and BP can be excited to their conduction bands, respectively. As a result of the Fermi level alignment at the BP-MoS<sub>2</sub> junction, a type-II heterostructure is formed with the valence band maximum of MoS<sub>2</sub> much lower than that of BP, leading to a much larger valence band offset than conduction band offset. Both photogenerated electron-hole pair dissociation and tunneling-mediated interlayer recombination between majority carriers at bottom (top) of the conduction (valence) band of MoS<sub>2</sub> (BP) are expected to contribute the photocurrent generation at the BP-MoS<sub>2</sub> junction. However, the recombination induced photocurrent response has an opposite photocurrent polarity in the junction region compared to the measured photocurrent signals. Therefore, photogenerated electron-hole pair dissociation becomes important. There are two pathways that can separate a photogenerated electron-hole pair at the BP-MoS<sub>2</sub> junction: 1) Photogenerated holes in MoS<sub>2</sub> drift to BP since the valence band maximum of MoS<sub>2</sub> is much lower than that of BP and 2) photogenerated electrons flow either from BP to MoS<sub>2</sub> or from MoS<sub>2</sub> to BP that depends on the polarity of the conduction band offset. The polarization-dependent photocurrent at the junction area is a competitive effect between BP and MoS<sub>2</sub>. In this typical device, the first pathway is dominant under the illumination of 532 nm laser. Photogenerated holes in the valence band of MoS<sub>2</sub> can flow to BP through a large band offset across the sharp interface, leading to strong photocurrent response. Indeed, this expectation has been confirmed by our polarization-dependent photocurrent measurements, where the photocurrent response at the MoS<sub>2</sub>-BP junction is polarized to the direction perpendicular to the MoS<sub>2</sub> channel. This is similar to the phenomenon observed at MoS<sub>2</sub>-metal junctions, where the maximum photocurrent response occurs for the light polarized perpendicularly to the MoS<sub>2</sub> channel when incident photon energy is above its band gap due to photovoltaic effect.<sup>31</sup>

Upon illumination of 1550 nm (0.8 eV) laser, the photocurrent signals primarily result from the direct band gap transition in BP since the incident photons cannot provide enough energy to excite electrons of MoS<sub>2</sub> from its valence band to its conduction band. Under this circumstance, the second pathway will become important (Figure 4h). Moreover, the photocurrent signals induced by two different pathways have the same polarity (Figure 4a and 4c), suggesting electrons flow from BP to MoS<sub>2</sub> in the second pathway. In addition, the maximum photocurrent response occurs when the incident light is polarized along the direction of electrode edges at the BP side (90°), which follows the polarization dependence of photocurrent response at the BP-metal junctions (Figure 4e and 4f). This further confirms that the photocurrent response at the BP-MoS<sub>2</sub> junction primarily results from the photogenerated electrons in BP. All the devices we tested display the same polarization dependency in the junction area

under 1550 nm illumination. Although photothermoelectric effect also contributes to the photocurrent generation, this effect is only expected to play a negligible role.<sup>6</sup> Another issue to consider is that the absorption of BP is polarization-sensitive depending on its crystal axis.<sup>30, 32</sup> However, in our experiment, the polarization directions that generate the maximum photocurrent signals in the junction region are different for 532 nm and 1550 nm illumination, whereas the BP crystal axis orientation stays the same. This result may indicate that the direction-dependent absorption of BP is not likely a dominant factor that determines the photocurrent polarization dependence at the MoS<sub>2</sub>-BP junction.

## Conclusions

To sum up, we fabricated a vertical heterostructure based on BP and MoS<sub>2</sub> flakes. This structure displays strong current rectifying characteristics similar to a conventional p-n junction at zero gate bias. The photocurrent generation mechanisms at the BP-MoS<sub>2</sub> p-n heterojunction is further investigated by gate-, wavelength-, and polarization-dependent scanning photocurrent microscopy. When the incident photon energy is above the direct band gap of MoS<sub>2</sub>, the photocurrent generation in the junction region depends on a competitive effect between BP and MoS<sub>2</sub>. In contrast, if the incident photon energy is below the band gap of MoS<sub>2</sub> but above the band gap of BP, the photocurrent response at the p-n junction primarily results from the direct band gap transition in BP. Our studies suggest that we may develop high-performance optoelectronic devices by further optimizing the junction structure and improve light-matter interactions by changing its polarization.

## Acknowledgements

This work was supported by the National Science Foundation (ECCS-1055852 and CBET-1264982 to YX; ECCS-1128297 and DMR-1308436 to ZZ).

## Notes and references

1. W. J. Yu, Y. Liu, H. L. Zhou, A. X. Yin, Z. Li, Y. Huang and X. F. Duan, *Nat Nanotechnol*, 2013, **8**, 952-958.
2. Y. Li, F. Qian, J. Xiang and C. M. Lieber, *Materials today*, 2006, **9**, 18-27.
3. H. Fang, C. Battaglia, C. Carraro, S. Nemsak, B. Ozdol, J. S. Kang, H. A. Bechtel, S. B. Desai, F. Kronast, A. A. Unal, G. Conti, C. Conlon, G. K. Palsson, M. C. Martin, A. M. Minor, C. S. Fadley, E. Yablonovitch, R. Maboudian and A. Javey, *Proceedings of the National Academy of Sciences*, 2014, **111**, 6198-6202.
4. W. J. Zhang, C. P. Chuu, J. K. Huang, C. H. Chen, M. L. Tsai, Y. H. Chang, C. T. Liang, Y. Z. Chen, Y. L. Chueh, J. H. He, M. Y. Chou and L. J. Li, *Sci Rep*, 2014, **4**, 3826.
5. D. Jariwala, V. K. Sangwan, L. J. Lauhon, T. J. Marks and M. C. Hersam, *Acs Nano*, 2014, **8**, 1102-1120.

6. C. H. Lee, G. H. Lee, A. M. van der Zande, W. C. Chen, Y. L. Li, M. Y. Han, X. Cui, G. Arefe, C. Nuckolls, T. F. Heinz, J. Guo, J. Hone and P. Kim, *Nat Nanotechnol*, 2014, **9**, 676-681.
7. L. Britnell, R. M. Ribeiro, A. Eckmann, R. Jalil, B. D. Belle, A. Mishchenko, Y. J. Kim, R. V. Gorbachev, T. Georgiou, S. V. Morozov, A. N. Grigorenko, A. K. Geim, C. Casiraghi, A. H. Castro Neto and K. S. Novoselov, *Science*, 2013, **340**, 1311-1314.
8. A. Kumar, J. Kumar and P. K. Ahluwalia, *AIP Conference Proceedings*, 2012, **1447**, 1269-1270.
9. Q. H. Wang, K. Kalantar-Zadeh, A. Kis, J. N. Coleman and M. S. Strano, *Nat Nanotechnol*, 2012, **7**, 699-712.
10. A. M. Jones, H. Yu, J. S. Ross, P. Klement, N. J. Ghimire, J. Yan, D. G. Mandrus, W. Yao and X. Xu, *Nat Phys*, 2014, **10**, 130-134.
11. D. Jariwala, V. K. Sangwan, C.-C. Wu, P. L. Prabhuram, M. L. Geier, T. J. Marks, L. J. Lauhon and M. C. Hersam, *Proceedings of the National Academy of Sciences*, 2013, **110**, 18076-18080.
12. R. Cheng, D. Li, H. Zhou, C. Wang, A. Yin, S. Jiang, Y. Liu, Y. Chen, Y. Huang and X. Duan, *Nano Letters*, 2014, **14**, 5590-5597.
13. Y. X. Deng, Z. Luo, N. J. Conrad, H. Liu, Y. J. Gong, S. Najmaei, P. M. Ajayan, J. Lou, X. F. Xu and P. D. Ye, *Acs Nano*, 2014, **8**, 8292-8299.
14. M. M. Furchi, A. Pospischil, F. Libisch, J. Burgdorfer and T. Mueller, *Nano Letters*, 2014, **14**, 4785-4791.
15. M. Buscema, D. J. Groenendijk, S. I. Blanter, G. A. Steele, H. S. J. van der Zant and A. Castellanos-Gomez, *Nano Letters*, 2014, **14**, 3347-3352.
16. T. Hong, B. Chamlagain, W. Lin, H. J. Chuang, M. Pan, Z. Zhou and Y. Q. Xu, *Nanoscale*, 2014, **6**, 8978-8983.
17. L. K. Li, Y. J. Yu, G. J. Ye, Q. Q. Ge, X. D. Ou, H. Wu, D. L. Feng, X. H. Chen and Y. B. Zhang, *Nat Nanotechnol*, 2014, **9**, 372-377.
18. H. Liu, A. T. Neal, Z. Zhu, Z. Luo, X. F. Xu, D. Tomanek and P. D. D. Ye, *Acs Nano*, 2014, **8**, 4033-4041.
19. Y. Takao and A. Morita, *Physica B & C*, 1981, **105**, 93-98.
20. M. Baba, F. Izumida, A. Morita, Y. Koike and T. Fukase, *Jpn J Appl Phys*, 1991, **30**, 1753-1758.
21. Y. Akahama, S. Endo and S. Narita, *J Phys Soc Jpn*, 1983, **52**, 2148-2155.
22. A. Morita, *Appl Phys a-Mater*, 1986, **39**, 227-242.
23. J. Qiao, X. Kong, Z.-X. Hu, F. Yang and W. Ji, *Nature Communications*, 2014, **5**, 4475.
24. M. Engel, M. Steiner and P. Avouris, *Nano Letters*, 2014, **14**, 6414-6417.
25. W. Choi, M. Y. Cho, A. Konar, J. H. Lee, G. B. Cha, S. C. Hong, S. Kim, J. Kim, D. Jena and J. Joo, *Advanced Materials*, 2012, **24**, 5832-5836.
26. O. Lopez-Sanchez, D. Lembke, M. Kayci, A. Radenovic and A. Kis, *Nat Nanotechnol*, 2013, **8**, 497-501.
27. H. Asahina, K. Shindo and A. Morita, *J Phys Soc Jpn*, 1982, **51**, 1193-1199.
28. C.-C. Wu, D. Jariwala, V. K. Sangwan, T. J. Marks, M. C. Hersam and L. J. Lauhon, *The Journal of Physical Chemistry Letters*, 2013, **4**, 2508-2513.
29. V. Klee, E. Preciado, D. Barroso, A. E. Nguyen, C. Lee, K. J. Erickson, M. Triplett, B. Davis, I. H. Lu, S. Bobek, J. McKinley, J. P. Martinez, J. Mann, A. A. Talin, L. Bartels and F. Léonard, *Nano Letters*, 2015, **15**, 2612-2619.
30. X. Wang, A. M. Jones, K. L. Seyler, V. Tran, Y. Jia, H. Zhao, H. Wang, L. Yang, X. Xu and F. Xia, *Nat Nanotechnol*, 2015, **10**, 517-521.
31. T. Hong, B. Chamlagain, S. Hu, S. M. Weiss, Z. Zhou and Y.-Q. Xu, *Acs Nano*, 2015, **9**, 5357-5363.
32. H. Yuan, X. Liu, F. Afshinmanesh, W. Li, G. Xu, J. Sun, B. Lian, A. G. Curto, G. Ye, Y. Hikita, Z. Shen, S.-C. Zhang, X. Chen, M. Brongersma, H. Y. Hwang and Y. Cui, *Nat Nanotechnol*, 2015, **10**, 707-713.